ANNUAL REVIEWS

Annual Review of Nuclear and Particle Science

Fundamental Neutron Physics at Spallation Sources

Nadia Fomin,[1] Jason Fry,[2] Robert W. Pattie Jr.,[3] and Geoffrey L. Greene[1]

[1]Department of Physics and Astronomy, University of Tennessee, Knoxville, Tennessee, USA; email: nfomin@utk.edu

[2]Department of Physics, Geosciences, and Astronomy, Eastern Kentucky University, Richmond, Kentucky, USA

[3]Department of Physics and Astronomy, East Tennessee State University, Johnson City, Tennessee, USA

Annu. Rev. Nucl. Part. Sci. 2022. 72:151–76

The *Annual Review of Nuclear and Particle Science* is online at nucl.annualreviews.org

https://doi.org/10.1146/annurev-nucl-121521-051029

Keywords

neutron β decay, hadronic weak interaction, neutron electric dipole moment, time-reversal symmetry violation, spallation neutron sources

Abstract

Low-energy neutrons have been a useful probe in fundamental physics studies for more than 70 years. With advances in accelerator technology, many new sources are spallation based. These new, high-flux facilities are becoming the sites for many next-generation fundamental neutron physics experiments. In this review, we present an overview of the sources and the current and upcoming fundamental neutron physics programs.

Contents

1. INTRODUCTION

The neutron was discovered as a fundamental particle in 1932. Shortly thereafter, its mass was measured well enough to show that a free neutron would undergo β decay, instead of a bound state of a proton and electron, as Rutherford (1) first supposed. The earliest experiments involving neutrons used nuclear reactions as neutron beams, until the graphite reactor in Tennessee, USA, became available in the late 1940s. The first fundamental neutron physics experiments measured the lifetime of the free neutron (2) and the electric dipole moment (EDM) of the neutron (nEDM) (3). Both classes of experiments are still being conducted around the world.

Fermi (4) was the first to formalize the weak interaction with a charged current (V), including Pauli's proposed new particle, the neutrino, necessary for energy conservation (5). Some kind of weak interaction was required to explain the long lifetimes of certain processes, including the neutron lifetime, which, at ~15 min, was much longer than anything that could be derived from strong or electromagnetic couplings. Fermi's formulation of β decay had zero range and did not have a mediator. Heavy mediator particles (bosons), including charged and neutral interactions, were introduced later (6) to explain flavor-changing processes as well as processes with charge exchange. The discovery of parity violation led to the introduction of equal parts of axial and vector currents by Feynman & Gell-Mann (7) in the late 1950s. The inclusion of both currents would become part of the Standard Model (SM) proposed by Glashow et al. (8). However, experimental observations suggested that g_A is not equal to g_V, and the strengths of these couplings are an active area of research today.

Fundamental symmetries is the subfield of experimental nuclear physics research that continues to investigate the weak interaction with neutrons. Neutron β decay experiments are discussed in Section 3.1. These measurements fall into two classes: measurements of the neutron lifetime and correlation parameters of neutron β decay products. Both are necessary to disentangle g_A and g_V and look for physics beyond the Standard Model (BSM). Low-energy neutrons have been used to map the hadronic weak interaction (HWI); recently, great progress has been made at the Spallation Neutron Source (SNS) (9, 10). Finally, researchers measuring the nEDM have been searching for a new source of *CP* violation for almost 80 years, and the next generation of experiments is under vigorous development.

Spallation and reactor sources produce continuous spectra of neutron energies. A thermal neutron has an energy of 25 meV, a velocity of 2,200 m s^{-1}, and a characteristic wavelength of 1.8 Å. Most nuclear physics experiments are done with cold neutrons (50 μeV < E < 25 meV) or

ultracold neutrons (UCNs; $E < 340$ neV). This is because it is often advantageous for the neutron to spend as much time in the experimental apparatus as possible. For example, in neutron decay experiments, the decay probability increases with the time neutrons spend in the apparatus. Some fundamental physics experiments utilize epithermal neutrons ($0.025\ \text{eV} < E < 1\ \text{eV}$) to access certain amplifications or resonances in neutron interactions with matter. Another feature of spallation sources is that the high-energy tail from eV–MeV neutron energies can be used to probe sharp resonances in heavy nuclei, as discussed in Section 3.2.2.

While the focus of this review is on fundamental physics at spallation sources, which are becoming more prevalent across the globe, for decades research reactors were the workhorse of neutron sources. Foundational neutron physics research was carried out at a research reactor in Munich, Germany (FRM-I, also known as the Atomic Egg), that formed the basis for future designs (11). Additionally, many of today's neutron scattering length data still come from those early measurements. FRM-II is now up and running, with the potential to provide UCNs for fundamental physics research in the future (12). The field of neutron interferometry was developed at research reactors, and its experiments and methods are well described in a recent book by Rauch & Werner (13). An overview of experimental programs leading up to the 1990s can be found in a book by Byrne (14), and a book by Krupchitsky (15) covers polarized beams of slow neutrons in fundamental neutron physics. The cold neutron and UCN facilities at Institut Laue-Langevin (ILL) in France have been and continue to be the home to many fundamental physics experiments (16, 17). The NIST Center for Neutron Research has been and still is the site of cutting-edge neutron interferometry research (18, 19) as well as fundamental neutron physics β decay research (20–24). In the past, high-energy neutron sources were also used to measure neutron cross sections and reactions as well as neutron polarizability. These high-energy, unmoderated neutron sources (25–28) are still in use today, including for nuclear physics studies, but are outside the scope of this review. Finally, promising fundamental physics experiments with neutrinos have begun to be carried out at spallation neutron sources (29).

2. SPALLATION SOURCES

2.1. General Principles

The earliest neutron sources used for experiments were reactions such as $\alpha + \text{Be} \rightarrow \text{C} + n$. The first nuclear research reactors came online in the late 1940s and early 1950s. They rely on neutrons liberated by fission from heavy atoms, typically uranium. Spallation sources can liberate neutrons from a wider variety of heavy atoms. In general, neutron production from spallation employs a pulsed, high-energy beam of protons (or hydrogen ions) that strikes a target of neutron-rich material to release neutrons, creating a few to up to ~40 neutrons per proton. Other particles are released and produced as part of this process, but they are either used for other physics studies or easily shielded. The most common spallation target material has been tungsten, but others have been employed as well (**Table 1**).

Once neutrons are liberated from the target nucleus, they can be moderated or slowed down via a few centimeters of hydrogen, deuterium, or other moderating materials (see **Table 1** and the description of sources in Section 2.2, below). Some target stations have a reflecting material (such as beryllium) to help the moderation process. Moderated neutrons are then transported down neutron guides to dedicated beamlines and instruments.

Most nuclear physics experiments that use low-energy neutrons are statistically limited by neutron intensity and thus require the highest possible flux, that is, the cold neutron flux available at the end of a dedicated neutron guide. For many experiments involving parity violation, a desired figure of merit is roughly the flux weighted by the neutron polarization. In general, the highest-flux

Table 1 Operating parameters for existing and upcoming spallation neutron sources with fundamental physics programs

Source	Repetition rate	Maximum power	Moderators[a]	Pulse length	Target	Proton energy
SNS	60 Hz	1.4 MW	H, H_2O	<1 ms	Hg	1.3 GeV
LANSCE	20 Hz	0.8 MW	Multiple	625 μs	W	800 MeV
ESS	14 Hz	5.0 MW	H	2.86 ms	W	2.0 GeV
SINQ	Continuous	~1 MW	H_2, D_2O	NA	Pb	590 MeV
JSNS	25 Hz	1.0 MW	H	1 μs	Hg	3.0 GeV
CSNS	25 Hz	0.5 MW (final)	Multiple	0.5 ms	W	1.6 GeV

[a]When H is used for the moderators, it is typically supercritical hydrogen.

Abbreviations: CSNS, China Spallation Neutron Source; ESS, European Spallation Source; JSNS, Japan Spallation Neutron Source; LANSCE, Los Alamos Neutron Science Center; NA, not applicable; SINQ, Swiss Spallation Source; SNS, Spallation Neutron Source.

research reactors provide more intense neutron beams than do the highest-flux spallation sources. However, this difference is usually not large enough to be compelling, and source selection is more often determined by the availability of beam time and/or facility infrastructure. The primary advantage for experiments done at spallation sources is the well-known time structure of the beam. A pulsed source has precise timing, which can be used to easily analyze the energy dependence either of the neutron beam itself or of the background signal, which is important for possible systematic effects. Additionally, the pulsed structure of the neutron beam allows the beam phase space to be shaped by use of time-dependent neutron optical components. The pulsed nature of most spallation sources may provide an additional advantage (30) for polarized neutron studies.

The process of creating UCNs is somewhat different. It is generally difficult to efficiently extract UCNs directly from neutron guides that directly view in-pile cold sources at either reactors or spallation sources. Instead, one of two alternate strategies is currently favored to provide intense sources of UCNs. In the first, a UCN converter consisting of very cold superfluid liquid helium ($T < 1$ K) is illuminated by a cold neutron beam with a characteristic wavelength of 8.9 Å. Neutrons with this energy may scatter off single phonons in the helium, resulting in residual energies characteristic of UCNs (31). Such UCN sources are equally well suited for reactors or spallation sources and are particularly well suited for experiments that can be carried out within the liquid helium converter volume, such as the search for an EDM (32). In the second strategy, a UCN converter [typically solid deuterium (SD_2)] is placed in the vicinity of a cold neutron moderator and the UCNs are extracted to an external experiment. Such sources are challenging because of the need to place a cryogenic moderator close to the neutron source (either reactor or spallation). Because spallation sources typically produce a much lower thermal load than reactors, this strategy is favored at spallation sources. Indeed, several of the most intense current sources of UCNs (33–36) are based on dedicated spallation targets coupled closely to liquid deuterium converters. The spallation targets used in these sources are typically rather low power but couple very well to the UCN converter.

2.2. Overview of Cold Neutron Sources

Spallation sources have become more prevalent in recent decades as accelerator technology has developed (see **Figure 1** for the geographic locations of spallation sources with fundamental physics programs around the world). Spallation sources are also attractive from the point of view of safety because they are not subject to the strict licensing requirements that apply to reactor sources. Most sources have a fairly similar design, with a pulsed ion beam incident on a neutron heavy target. The spallation process creates a large charged-particle background in addition to liberating neutrons,

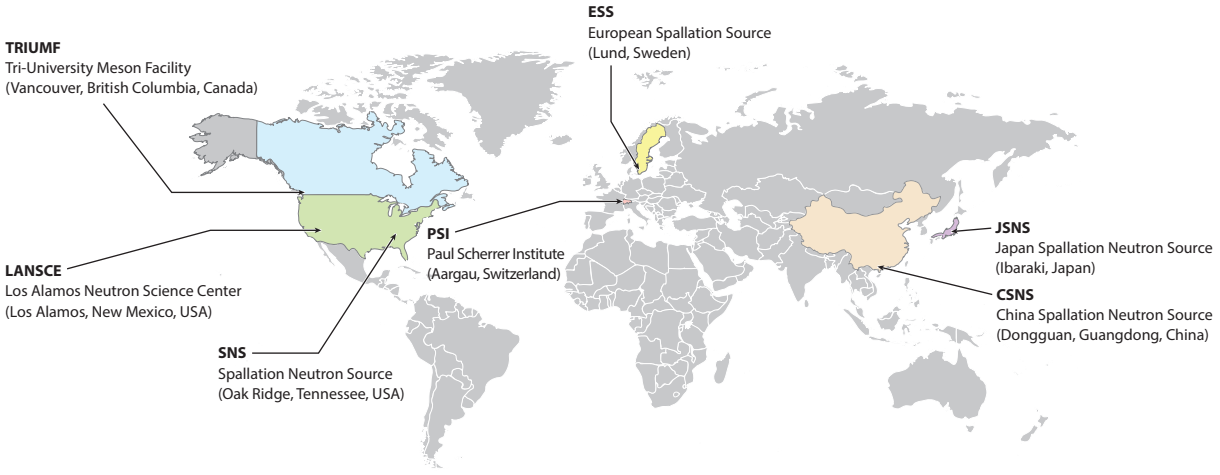

Figure 1

Spallation neutron sources around the world that offer user facilities for fundamental physics.

requiring significant shielding of the target. Moderators are employed to produce a desired energy spectrum (for fundamental neutron experiments, a cold neutron spectrum is normally preferred). Typically, several beamlines view a single moderator. The Swiss Spallation Source (SINQ) at the Paul Scherrer Institute (PSI) is different and is discussed separately (see Section 2.2.4). **Table 1** summarizes the relevant parameters for existing and future spallation sources.

2.2.1. Spallation Neutron Source. Currently, the First Target Station (FTS) at the SNS at Oak Ridge National Laboratory in Tennessee, USA, is the most intense pulsed neutron source in the world. Unlike many other spallation sources, the FTS employs a rotating liquid mercury target. The target material is circulated to dissipate heat from the incident proton beam. This end station was optimized for the production of thermal neutrons, which are most useful for resolving atomic-scale details. Plans for the Second Target Station (STS) have received CD-1 (Critical Decision) approval from the US Department of Energy, allowing for the release of project engineering and design funds, if available. The STS will focus on addressing global needs for cold neutrons. The SNS proton source will receive a power upgrade, and every fourth pulse (15 Hz) will be sent to the STS's solid, rotating tungsten target. Current plans include two cold moderators and one ambient moderator, a proton pulse of 0.75 μs with an energy per pulse of 47 kJ, and the potential for 22 instruments. The proton source power upgrade will allow the FTS to maintain the same power per second. Out of more than 20 existing beamlines at the FTS, one (the FnPB) is dedicated to fundamental neutron physics (for details, see 37). The physics program on the FnPB began with HWI studies of the NPDGamma (38) and n–^{3}He (10) experiments. Currently, the Nab experiment (39) is commissioning and will be followed by the nEDM@SNS experiment (32, 40).

2.2.2. Los Alamos Neutron Science Center. Los Alamos Neutron Science Center (LANSCE) is home to two neutron sources, both of which are driven by the 800-MeV pulsed proton beam from the LANSCE accelerator. The pulses start at 625 μs and are then injected into the proton storage ring, where they are accumulated and compressed into pulses approximately 250 ns wide. The first neutron source is a high-energy source at the Weapons Neutron Research Facility, which produces fast neutrons (100 keV $< E <$ 800 MeV) by use of an unmoderated

target. The low-energy source at the Lujan Neutron Scattering Center provides neutron beams from subthermal energies up to 100 keV. The proton beam is pulsed at 20 Hz incident on a tungsten target. Flight Path 12 was constructed in 2003 (41) as a beamline dedicated to nuclear physics experiments; NPDGamma was the first to take a data set (42). In 2022, a next-generation spallation neutron target/moderator/reflector/shield assembly will begin installation. The goal is to improve performance in the intermediate energy (keV–MeV) range and increase time resolution, which will be useful for a number of upcoming nuclear physics experiments.

2.2.3. Japan Spallation Neutron Source. The Japan Spallation Neutron Source (JSNS) is housed in the Material and Life Science Experimental Facility (MLF) on the Japan Proton Accelerator Research Complex (J-PARC) campus. Protons are accelerated through a linear accelerator to 400 MeV and then fed into the Rapid Cycling Synchrotron, where they are further accelerated to 3 GeV. The protons are incident on a cycling mercury target, and the spalled neutrons interact with liquid hydrogen moderators (coupled, decoupled, and poisoned) and beryllium reflectors. The neutrons are delivered to 23 beamlines at the MLF. Fundamental neutron physics is conducted on three beamlines: BL04 ANNRI (Accurate Neutron–Nucleus Reaction Measurement Instrument), BL05 NOP (Neutron Optics and Fundamental Physics), and BL10 NOBORU (Neutron Beamline for Observation and Research Use). The neutron lifetime experiment discussed in Section 3.1.1.4 is conducted on BL05, and the time-reversal violation (TRV) experiments discussed in Section 3.2.2 will be conducted on BL04 and BL10.

2.2.4. Swiss Spallation Source. SINQ differs from the other sources under discussion here, and as such, direct comparisons in **Table 1** are difficult to make. SINQ is a continuous (rather than pulsed) spallation neutron source, driven by a 590-MeV proton accelerator. The initial proton beam has a current of 1.3 mA and a time structure of 51 MHz, but the time structure is lost following impact on the lead spallation target and moderation (43). The proton beam, at 0.75 MW in continuous mode, is the most powerful in the world. SINQ has been in operation since 1997; an upgrade performed between 2017 and 2020 focused on the guide system (44). The UCN source does not use the main SINQ spallation source but rather extracts a low-current proton beam to a dedicated spallation target, discussed in more detail in Section 2.3.1.2.

2.2.5. China Spallation Neutron Source. The China Spallation Neutron Source (CSNS) is an accelerator-based neutron source in Dongguan, Guangdong Province, that operates under the direction of the Institute of High Energy Physics of the Chinese Academy of Sciences (45, 46). The facility contains a proton linear accelerator coupled to a rapid cycling synchrotron that delivers 1.6-GeV protons to the target station (47). The target station consists of a solid tungsten target and a target cooling system, which includes deuterium, liquid hydrogen, carbon, and water moderators. Neutrons will be delivered to a total of 18 planned instruments, 3 of which were operational when the neutrons were first created in 2017. The design goal of phase I, 100 kW, was achieved in February 2020, and progress toward the goals of phase II continues. Beamline 12 is equipped to eventually pursue experimental research on neutron lifetime and decay (48).

2.2.6. European Spallation Source. The European Spallation Source (ESS) in Lund, Sweden, is nearing completion. The ESS aims for the highest peak intensity among spallation sources, combined with a long pulse structure (3 ms) and a power of 5 MW. Up to 48 beam ports can be accommodated. Currently, there is no approved beamline for fundamental neutron physics, but the possibility remains open.

2.2.7. Other spallation sources without fundamental physics programs. Of course, other spallation sources exist without fundamental physics programs as defined in this review. ISIS in the

United Kingdom, a world-leading center in neutron scattering research, has recently used neutron spin echo to investigate exotic spin-dependent interactions (49), with the possibility of placing limits on other exotic interactions. The spallation source at the Research Center for Nuclear Physics in Japan (RCNP) produces a white neutron beam and houses an irradiation program for nuclear physics. The now-decommissioned sources at IPNS (Intense Pulsed Neutron Source) and RCNP/KEK enabled early studies of UCN production and p-wave resonances in heavy nuclei, respectively. In addition, several university-based spallation sources serve as testing grounds for numerous physics studies.

2.3. Ultracold Neutron Sources

Cold neutrons can be cooled from 60 K to below 3.5 mK through scattering interactions on solid or liquid cryogenic converters, resulting in UCNs. At this energy, the neutrons' de Broglie wavelength is sufficiently large that they can coherently scatter from a collection of nuclei in solids, acting as an effective potential barrier or Fermi potential, V_F, on the order of 100 neV. ^{58}Ni is typically quoted as having the greatest Fermi potential at $V_F^{^{58}\mathrm{Ni}} = 358$ neV. Operationally, this means that UCNs can be totally externally reflected from material walls for all angles of incidence when their kinetic energy is below the material's Fermi potential (31, 50). Experiments have exploited this feature to transport UCNs 10–20 m away from the source in material guides such as a noninteracting ideal gas and confine them in material traps for hundreds to thousands of seconds. These properties enable experiments to perform measurements of the neutron lifetime and β decay correlation parameters (51, 52), place limits on the nEDM (53, 54), and observe gravitational quantum states (55).

At the energy scale of UCNs, the interactions with gravity and magnetic fields become relevant and, in some cases, become useful experimental tools. UCNs in the Earth's gravitational field experience a potential energy difference of $\sim$100 neV m^{-1}, meaning that, on average, a UCN can rise only 2 m. Dropping a UCN by 1 m will sufficiently increase its kinetic energy, allowing UCNs to pass through materials such as gas detector windows. Magnetic fields interact with the magnetic moment of the neutron, creating a potential $-\mu_n \cdot \mathbf{B}/|\mathbf{B}| \approx 60$ neV T^{-1}. A population of UCNs can be effectively 100% polarized by being passed through a magnetic field of 6–7 T, which provides a 360–420-neV potential barrier for one spin state.

2.3.1. Existing ultracold neutron sources at spallation targets. UCN sources are operated at facilities that can provide a large flux of cold neutrons, such as reactors and spallation sources. The discussion in this section focuses on the operation of UCN sources at spallation sources; however, many of the processes are similar at a reactor source, and a full discussion of all UCN sources can be found elsewhere (56). The production of UCNs at spallation sources requires a large flux of cold neutrons to be cooled from a few to $\sim 10^{-13}$ MeV. Depending on the facility, the entire spallation target or a portion of it is surrounded by room-temperature or cryogenic neutron reflectors and thermal moderators, which are designed to trap and thermalize a fraction of the spallation neutron flux. The mechanical and thermal details of the reflectors and moderators depend on the conversion material used in the final step to reduce the energy of cold neutrons to the UCN regime. Materials such as SD_2, solid oxygen, and liquid helium have been studied or are in use as the conversion medium in UCN sources (56). The design goal is to maximize the overlap between the neutron energy spectrum produced by thermalizing the spallation neutrons with the moderator and the energy-dependent UCN production cross section of the converter medium.

2.3.1.1. Los Alamos Neutron Science Center. LANSCE hosts an SD_2-based UCN source (**Figure 2*a***), which began operation in 2004 (33) and underwent an upgrade between 2014 and

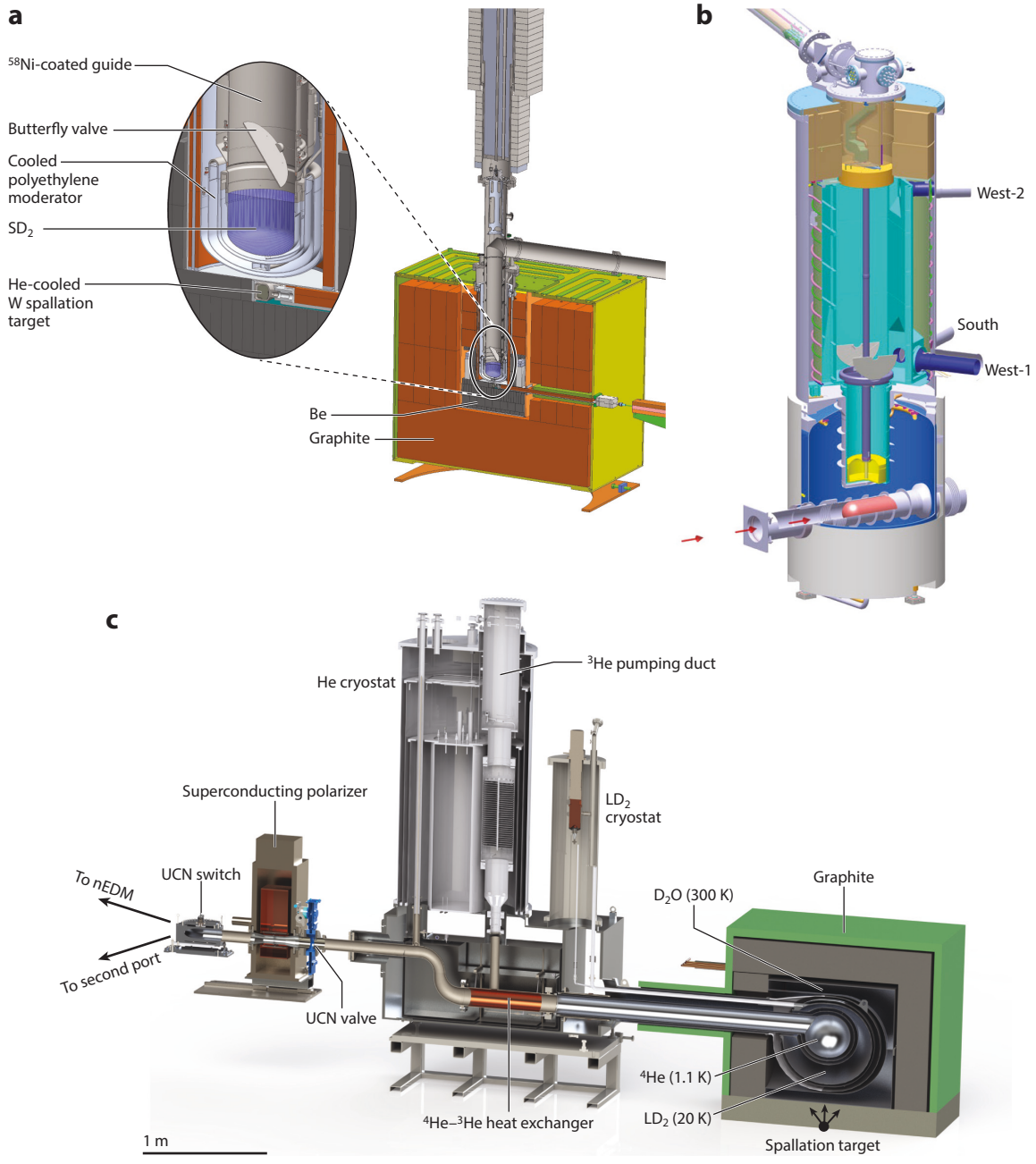

Figure 2

Engineering renderings of the UCN sources at (*a*) LANSCE, (*b*) PSI, and (*c*) TRIUMF. Abbreviations: nEDM, electric dipole moment of the neutron; UCN, ultracold neutron. Panel *a* adapted with permission from Reference 34. Panel *b* adapted with permission from Reference 35. Panel *c* adapted with permission from Reference 57.

2017 (34). This source was constructed to support the UCNA experiment, which completed data taking in 2013 (52) and has since expanded operation to host the UCNτ experiment (51); a future room-temperature nEDM search, UCNProbe (58); and several material studies and detector development projects. Two main beamlines from the source can host multiple experiments simultaneously.

The LANSCE accelerator delivers a time-averaged proton current of 10 μA to the helium-cooled tungsten target. Protons are delivered in several pulses with a repetition rate of 20 Hz over a 0.2-s window. When the accelerator is operating in production mode, one burst is delivered every 5 s. During this period, the butterfly valve is open, allowing converted UCNs to escape, but it is closed between bursts to prevent UCNs from returning to the SD_2. A graphite and beryllium reflector concentrates a fraction of the spallation neutrons through a moderator of 45 K high-density polyethylene beads and a 4.5 K SD_2 crystal. UCN surfaces at the bottom of the source are coated with ^{58}Ni, and the guide system to the experiment hall is coated with NiP (59). The 1-m ascent from the SD_2 to the horizontal guides is designed to offset the 102-neV boost that the UCNs receive when exiting the SD_2. NiP-coated guides, with a Fermi potential of 212 neV, deliver UCNs with a cutoff velocity of 5.3 m s^{-1} and an internally measured unpolarized density of 180 UCNs cc^{-1} to the exit of the biological shielding.

2.3.1.2. Ultracold neutrons at the Paul Scherrer Institute. Another SD_2-based UCN source has been operating at PSI since 2011 (35, 36) (**Figure 2*b***). An average current of 2.5-mA, 590-MeV protons from the PSI cyclotron is incident on a "cannelloni"-type lead, Zircaloy, and D_2O spallation target for irradiation periods of up to 8 s. A 3,300-L, room-temperature (31°C), heavy-water moderator volume surrounding the target and converter volume thermalizes neutrons liberated in the spallation process (60). UCNs are then produced in a 5 K, 30-L SD_2 volume located inside the source vacuum vessel. Unlike the LANSCE source, the SD_2 acts as both a cold moderator and a UCN converter medium. Significant care is dedicated to slowly freezing the deuterium over several days into a near-perfect crystal and to maintaining an ortho-D_2 concentration of greater than 99% to optimize production. Several groups have observed the effect of the SD_2 crystal on production, and Anghel et al. (61) present a detailed report.

UCNs are vertically extracted from the source volume into the guide system through three ports; two are 1 m above the SD_2, and the other is 2.3 m above. A horizontal flapper valve is employed just below the lower two ports to isolate the SD_2 from the guide volume, preventing UCNs in the guide system from getting lost in the source. UCN shutters on each exit guide allow flexibility in operation by selecting a guide or set of guides to provide UCNs to (or condition the UCNs from) each irradiation period in the source storage volume before delivering them to an experiment. The differing heights of the extraction ports give experiments access to UCNs with different energy spectra due to the additional 130 neV of energy lost to gravity during the ascent. In 2017, a benchmark measurement using a 20-L standard storage volume was done at PSI. This measurement yielded a trappable density of 21.9 UCNs cm^{-3} (62)—the largest reported from the sources studied. Since becoming active, the source has supported various physics experiments, most notably a new determination of the upper limit on the nEDM using the RAL-Sussex-ILL apparatus (described in 63), which improved the previous limit by a factor of 1.7 (54).

2.3.1.3. TRIUMF UltraCold Advanced Neutron Source. TRIUMF, which produced its first UCN in 2017, hosts the TRIUMF UltraCold Advanced Neutron Source (TUCAN), which was constructed to support a future high-precision room-temperature nEDM search (57). An initial prototype source was built in collaboration with RCNP and transferred to TRIUMF. The design makes use of the superthermal process in liquid helium, where 8.9-Å neutrons downscatter to UCN energies by exciting a phonon in the liquid helium (50, 64). Spallation neutrons are reflected

and moderated by a combination of palladium, graphite, and heavy water around a water-cooled tungsten target. UCNs are extracted vertically from the liquid helium volume through a valve after a 60-s irradiation period, with the 450-MeV proton beam at an average current of 10 μA. This long irradiation approach is made feasible by cooling the liquid helium to below 1 K, suppressing any excitation modes that could upscatter UCNs. As a result, the storage time of UCNs in the source volume increased to 37 s, allowing a large UCN density to build up in the source prior to opening the valve. The density produced by this configuration was measured at 5.3 UCNs cm^{-3} in the 60-L guide volume.

The next phase of the TUCAN source will replace the vertical liquid helium vessel with a horizontal source (**Figure 2*c***). This upgrade is currently underway, with a planned completion date in 2022. It will significantly improve cooling to the cryostat, allowing the average proton current delivered to the target to increase from 10 μA to 40 μA (57). The upgrade will include a 20 K liquid deuterium cold moderator surrounded by a 300 K D_2O thermal moderator and palladium and graphite neutron reflectors. Estimates of this configuration suggest that the nEDM cells will be filled to a density of 33.4 UCNs cm^{-3} every 60 s of irradiation, enabling a 10^{-27} nEDM measurement every 400 running days. Additionally, the upgrade will support two beamlines; one will be dedicated to the nEDM search, and the other will become a user beamline capable of hosting next-generation lifetime, asymmetry, or gravity experiments with UCNs.

2.3.1.4. J-PARC pulsed source. UCNs are created at the J-PARC BL05 NOP beamline through the use of a Doppler shifter–type pulsed source (65) that is similar in concept to the Steyerl turbine at the ILL FP5 (Physique Fondamentale) (16). Very cold neutrons (VCNs) from the unpolarized branch of BL05 are directed into a focusing guide and then into the Doppler shift apparatus via a set of $m = 3.5$ multilayer, wideband, monochromatic mirrors. The VCNs are converted to UCNs by scattering from a NiC/titanium multilayer mirror mounted at the end of a rotor arm. The rotor assembly rotates at 2,000 rpm and is synced to the accelerator pulse timing, so that VCNs from every third pulse enter in phase with the rotor. Initial testing measured a product density of 1.4 UCNs cm^{-3}, which is sufficient for further testing and development of an nEDM search experiment.

2.3.2. Possible future ultracold neutron sources at spallation targets. The ESS is considering the inclusion of a fundamental physics beamline and a next-generation UCN source (for a full discussion of this possibility, see 66). Source designs are still being investigated for their compatibility with the facility's physics goals, but it is expected that the densities produced will be of order 10^3–10^4 UCNs cm^{-3}, significantly higher than densities at operating sources. Construction of such a source would enable nEDM, β decay, and UCN-based gravity experiments with unparalleled sensitivity.

2.3.3. Experiments with ultracold neutrons at spallation targets that are their own source. The preceding subsections discuss UCN sources where the neutrons must be extracted via a guide system to an experiment, but that is not necessarily required. As demonstrated by the NIST cryogenic neutron lifetime measurement, UCNs can be generated and stored in a liquid helium volume for times longer than the neutron's β decay lifetime, and the experiment and source can be colocated (67). The nEDM search at SNS will operate in this mode (68). UCNs will be produced through interaction of the cold neutron beam at the FnPB with a superfluid ^{4}He target, and the production volume will be the storage cell of the nEDM experiment. A deuterated polystyrene–coated storage chamber will be irradiated for a duration of several hundred seconds by cold neutrons from the FnPB moderator. Simulations predicted a trappable polarized density of ∼170 UCNs cm^{-3} to be produced each fill cycle, resulting in $\sim 10^6$ UCNs in storage volume (68).

This method benefits from eliminating all the transport losses and in-transit depolarization associated with the extracted source.

3. FUNDAMENTAL NEUTRON PHYSICS

Fundamental neutron physics experiments fall into several classes. As mentioned in Section 1, precision measurements of the neutron lifetime and correlation parameters in neutron β decay are still being carried out today. Attempts to measure a nonzero nEDM are ongoing, as the question of the observed matter/antimatter asymmetry of the Universe is one of the most intellectually compelling pursuits. Recently, significant progress has been made in studies of the HWI with cold neutrons, but more remains to be done. Finally, interest has reemerged in TRV searches complementary to searches for nonzero nEDMs. All of the efforts currently underway or planned for spallation sources are discussed in the following subsections.

3.1. Neutron Beta Decay

Neutron β decay is the archetype for all nuclear β decays. It is the simplest baryonic weak interaction process and serves as an important interaction to test our understanding of the SM. The sensitivity of neutron β decay to the SM and to BSM physics has been carefully studied and categorized (69, 70). Specifically, measurements of the neutron lifetime and β decay correlations allow a determination of V_{ud}, the *ud* quark mixing matrix element in the Cabibbo–Kobayashi–Maskawa (CKM) matrix. Such a determination can be compared with measurements of V_{us} and V_{ub} to provide a sensitive test of the unitarity of the CKM matrix. Because $V_{ud} > V_{us} > V_{ub}$, the uncertainty in the unitarity sum $V_{ud}^2 + V_{us}^2 + V_{ub}^2$ is dominated by the proportional uncertainty in V_{ud}. The unitarity of the CKM matrix is central to the SM. A violation of unitarity might result from right-handed currents, from other nonstandard couplings, from coupling to additional quark generations, or as a result of other exotic phenomena.

At tree level, the neutron decay rate, integrated over kinematic variables, is

$$\Gamma = \frac{1}{\tau_n} = \frac{f^R m_e^5 c^4}{2\pi^3 \hbar^7} |V_{ud}^2| (|g_V|^2 + 3|g_A|^2), \quad 1.$$

where f^R is a phase-space factor, m_e is the electron mass, and g_A and g_V are the axial-vector and vector coupling constants. An important input parameter into the SM is the ratio of the axial-vector constant to the vector coupling constant, $\lambda = g_A/g_V$. Using λ and the relationship between g_V and V_{ud}, we can rewrite the inverse of the neutron lifetime as

$$\frac{1}{\tau_n} \propto |V_{ud}|^2 |g_V|^2 G_F^2 \left(1 + 3|\lambda|^2\right), \quad 2.$$

where G_F is the Fermi weak coupling constant. By contrast, because the axial current is only partially conserved, the matrix element $\mathcal{M}_{GT}$ in the coupling $g_A \mathcal{M}_{GT}$ will vary across nuclei. The methods for extracting V_{ud} from $0^+ \rightarrow 0^+$ nuclear decays depend on quite different detailed nuclear and radiative corrections from the vector coupling, $g_V \mathcal{M}_F$, whereas a determination of V_{ud} from the neutron is easier to interpret because it is free from nuclear structure effects. To be competitive with nuclear extractions of V_{ud}, an uncertainty of $\tau_n \leq 0.3$ s of the neutron lifetime and a relative precision of $\Delta\lambda/\lambda \leq 3 \times 10^{-4}$ are required. With the most recent result from the UCNτ Collaboration reaching a statistical precision of 0.28 s (0.36 s overall) (51), we have entered what has previously been labeled the next generation of neutron β decay experiments.

In the following subsections, we discuss both sets of experiments, focusing on those at spallation facilities. The muddled nature of the current landscape of neutron β decay is well summarized

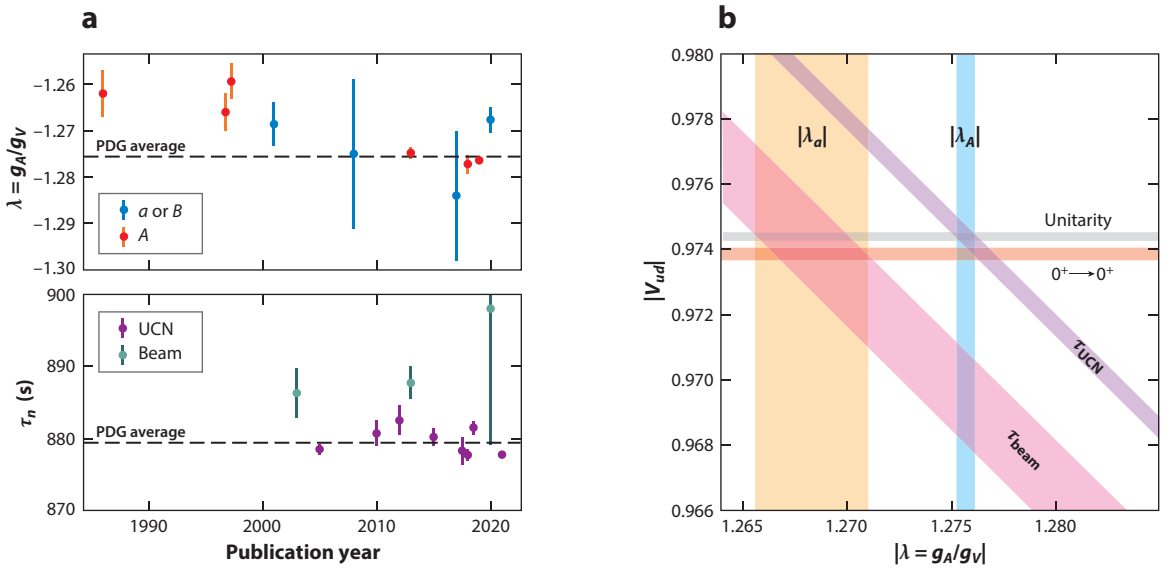

Figure 3

(*a*) (*Top*) $\lambda = g_A/g_V$ as a function of publication year. (*Bottom*) The same for the neutron lifetime. (*b*) V_{ud} as a function of $\lambda = g_A/g_V$. The diagonal stripes correspond to neutron lifetime extractions from the beam and storage (UCN) methods. The horizontal stripes represent the unitarity requirement as well as V_{ud} from a global $0^+ \rightarrow 0^+$ analysis (70). Abbreviations: PDG, Particle Data Group; UCN, ultracold neutron.

in **Figure 3**: The highest-precision results are not in agreement with CKM unitarity (71–74), there exists a 4σ neutron lifetime puzzle (20, 51, 75, 76), and λ determinations via different decay correlation parameters are also in tension. There is an opportunity for a great deal of experimental progress to help address this picture.

3.1.1. Neutron lifetime measurements. The first neutron lifetime measurement was performed at the Graphite Reactor at Oak Ridge National Laboratory, USA, in the late 1940s. The published result was approximately 30 min, much higher than more modern measurements of ~15 min (2). This result was quickly followed by a more precise measurement (77) from Canada, which yielded a value of 12.8 min with an uncertainty of 18%. Since then, there have been several attempts, primarily at reactors, to improve the precision of the value.

All measurements of radioactive lifetimes fall into two main categories. The first is referred to as the storage method. If the material's lifetime is comparable to the timescale of the experiment, then a measurement can be done directly, specifically by comparing the quantities of the material at two different times [$N(t) \propto N(0)e^{-t/\tau_n}$]. While this method is not a practical way to measure the lifetime of something like plutonium, it is well suited to the free neutron, whose lifetime is approximately 15 min. The second method is referred to as the beam method. It involves detecting decay products, dN/dt, and comparing them with the known quantity at a previous time, $N(t)$, via $dN(t)/dt \propto -N(t)/\tau_n$.

In the early 2000s, the precision of storage measurements reached 1 s, and upon reanalysis of old results, a disagreement emerged between storage and beam lifetime determinations. Additional storage measurements (51, 75, 76, 78) were carried out, and the most recent beam result (20) has been updated with an independent neutron detection efficiency determination (21), but the 4σ discrepancy remains to this day. It has not been resolved by the era of 1-s precision measurements,

but upcoming efforts aim to reach subsecond uncertainties, which may reveal systematics that were not previously considered or not properly taken into account.

3.1.1.1. Storage (ultracold neutron) measurements. The low kinetic energy of UCNs enables lifetime measurements on a trapped population using any combination of material wall, gravity, and magnetic fields. In this method, two approaches are possible, sometimes referred to as counting the living and counting the dead. The latter is similar to beam experiments in that the β decay products are counted and the exponential decay law is used to extract the lifetime. The rate of emitted electrons or protons that are counted is given by

$$R(t) \propto \frac{e^{-t/\tau_n}}{\tau_n}, \qquad 3.$$

where τ_n is the neutron's β decay lifetime. Ideally, this method enables a direct fit to the exponential decay of the event rate to extract the lifetime. Experiments such as PENeLoPE (79), HOPE (68), τSpect (80), and the NIST cryogenic lifetime (67) can be placed in this class. However, all of these experiments are or were at reactor facilities and are not discussed further in this review.

The more common approach is to count the surviving neutrons after storing them in the trap for a given time. One can then map the exponential decay curve by performing multiple measurements at various storage times. A more statistically optimized approach is to select two storage times, a short time t_s and a long time t_l, where the difference is $\Delta t = t_l - t_s = 2.2\tau$.[1] Then the lifetime is determined as

$$\tau_n = \frac{-\Delta t}{\ln\left(\frac{N_l}{N_s} \cdot \frac{N_{s0}}{N_{l0}}\right)}, \qquad 4.$$

where N_s and N_l are the neutrons counted after the short and long storage times, and N_{s0} and N_{l0} are normalization parameters to account for the variability of the initial number of neutrons in the trap at the beginning of each measurement cycle. Determining the lifetime from Equation 4 is an idealization because it assumes that β decay is the only way in which UCNs disappear from the trap. Thus, the main systematic of this type of experiment is understanding and limiting every possible non-β decay loss mechanism.

In general, the measured lifetime is the storage lifetime in the trap, which is a combination of all loss rates:

$$\tau_{\text{trap}}^{-1} = \tau_\beta^{-1} + \sum_i \tau_i^{-1}, \qquad 5.$$

where τ_β is the actual neutron β decay lifetime and τ_i are the storage lifetimes due to every loss channel. In the past, the correction between the trap and the β decay lifetime was 10–100 s. Modern storage experiments have reduced this correction to seconds or less. Over the past decade, many experiments of this type have produced results, which have been summarized by the Particle Data Group (81), but only the UCNτ experiment at the LANSCE UCN source is conducted at a spallation facility (51).

3.1.1.2. Beam methodologies for neutron lifetime experiments. The so-called beam method for the neutron lifetime requires detection of electrons, protons, or both from neutron β decay, as well as the determination of the density of neutrons in the fiducial decay volume. To date,

[1]The constant 2.2 is altered when the experimental signal-to-noise ratio is incorporated into the statistical optimization.

the approach that has produced the highest-precision results using this method is the Sussex-ILL-NIST beam method (20, 23, 82), named after the apparatus running at the NIST Center for Neutron Research. Here, protons are trapped from in-flight decays of cold neutrons within a fiducial volume. These protons are then directed to a silicon detector at an angle with respect to the neutron beam. The fluence of the neutron beam is monitored downstream with a dedicated apparatus. This experiment requires absolute proton and neutron counting and a high flux of cold neutrons that is typically available only at reactor-based sources. A program being developed at J-PARC is based on the use of a time-projection chamber as both the decay and the detection volume. This program is discussed further in Section 3.1.1.4, below.

3.1.1.3. UCNτ experiment at Los Alamos Neutron Science Center. To suppress or eliminate the corrections arising from UCN losses caused by their interaction with material surfaces, several experiments have investigated the use of magnetic confinement (67, 78, 80). The UCNτ experiment (**Figure 4**) used 5,000 permanent magnets arranged in a Halbach array to construct an asymmetric bowl with an inner surface field of 0.8 T. As a result of the $\mu_n \cdot \mathbf{B}$ interaction, low-field-seeking UCNs are repelled from the bottom of the bowl. UCNs with kinetic energy below 50 neV cannot ascend enough to escape the top of the bowl and are gravitationally trapped. The asymmetry in the bowl was implemented to prevent regular orbits, which would permit UCNs with energy above the trapping potential to remain in the trap for an intermediate length of time. A small trapdoor in the bottom of the magnetic bowl can be removed to fill the trap and then replaced during cleaning and storage. The surviving neutrons are counted after the storage period (10–5,000 s) by a ^{10}B-coated scintillator detector, called the dagger, that is lowered through the midplane of the trap. UCNs can be counted as a function of height by incrementally lowering the detector, which allows for an energy-dependent determination of the lifetime, mainly as a check on energy-dependent systematic effects. In 2021, UCNτ published (51) a result of $\tau_n = 877.74(\pm 0.28)_{\text{stat}}(^{+0.22}_{-0.16})_{\text{syst}}$, an improvement of roughly a factor of two over the previous most precise determination.

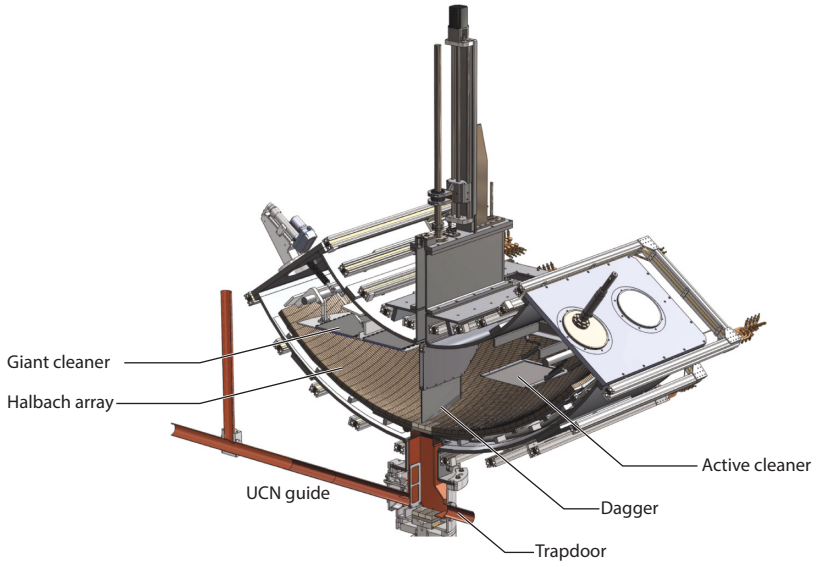

Figure 4

The UCNτ experimental apparatus (for details, see 51).

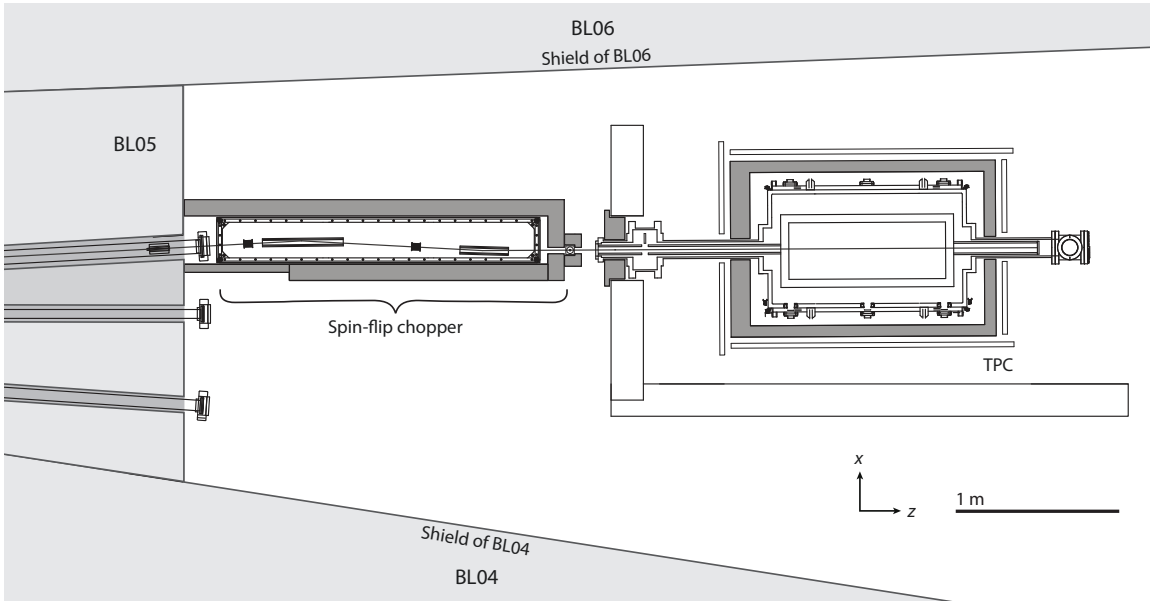

Figure 5

Schematic of the J-PARC lifetime apparatus (for details, see 85). Proton and neutron detection happens in situ in the TPC. Abbreviation: TPC, time-projection chamber. Figure adapted with permission from Reference 85.

3.1.1.4. J-PARC beam lifetime measurement. A new experiment utilizing the beam method has been under development for several years at BL05 NOP at the MLF in J-PARC (83–85) (**Figure 5**). This experiment employs a time-projection chamber to measure the neutron lifetime by detecting particles from two processes. The first is the neutron β decay itself, where the electron tracks are detected. The second is neutron capture on ^{3}He, used to monitor the neutron fluence in the time-projection chamber volume. Protons and tritium are detected from the $^3\mathrm{He}(n, p)^3\mathrm{H}$ reaction. The neutron lifetime is obtained via

$$\tau_N = \frac{1}{\rho\sigma_0 v_0}\left(\frac{S_{\mathrm{He}}/\epsilon_{\mathrm{He}}}{S_\beta/\epsilon_\beta}\right), \qquad 6.$$

where the S quantities are the numbers of events from each of the two processes and the ϵs are their efficiencies, ρ is the number density of the ^{3}He nuclei in the time-projection chamber, and $\sigma_0 v_0$ is the reaction rate. The approach is insensitive to γs, which is a big advantage. Backgrounds from cosmic rays and other sources are time independent, while the signals from neutron β decay are correlated with the time of flight, allowing for straightforward background subtraction. The sensitivity of this experiment is quickly growing, and is benefiting from source improvements as well.

3.1.2. Correlation parameter measurements. Neutron lifetime measurements are sensitive to the linear combination of the weak couplings g_A and g_V, whereas measurements of the decay correlation parameters isolate their ratio, g_A/g_V, also known as λ. The differential form of the β decay equation is (86)

$$\mathrm{d}W \propto \frac{1}{\tau} f(E_e)\left[1 + a\frac{\mathbf{p}_e \cdot \mathbf{p}_\nu}{E_e \cdot E_\nu} + b\frac{m_e}{E_e} + A\frac{\sigma_n \cdot \mathbf{p}_e}{E_e} + B\frac{\sigma_n \cdot \mathbf{p}_\nu}{E_\nu} + \ldots\right], \qquad 7.$$

where $\mathbf{p}_e$, $\mathbf{p}_p$, and $\mathbf{p}_\nu$ are the outgoing electron, proton, and neutrino momenta, respectively; σ_n is the neutron spin; and E_ν is the neutrino energy. $f(E_e)$ is in the familiar β energy spectrum. The

most frequently measured correlation parameters are all related to λ:

$$a = \frac{1-\lambda^2}{1+3\lambda^3}, \quad 8.$$

$$b = 0, \quad 9.$$

$$A = -2\frac{\lambda^2+\lambda}{1+3\lambda^3}, \quad 10.$$

$$B = 2\frac{\lambda^2-\lambda}{1+3\lambda^3}. \quad 11.$$

The uppercase parameters are spin dependent and require a polarized neutron beam, whereas the lowercase parameters are spin independent and require an unpolarized beam. For example, a is the correlation between the electron and neutrino momenta, and A is the correlation between the initial neutron spin and the direction of the outgoing electron. b, the Fierz interference term, corresponds to the deformation of the electron spectrum, compared with the SM prediction ($b = 0$ in the SM).

Until recently, determinations of λ were derived primarily from measurements of A, which requires a polarized source of neutrons and good knowledge of the polarization. The aCORN Collaboration (22) recently carried out a modern measurement of a. A more precise measurement of a, by the aSPECT Collaboration (87), yielded a λ value that was not in agreement with the result from the Particle Data Group (88). More recent A results from the UCNA and Perkeo III experiments can be found in References 52 and 87. **Figure 3** summarizes the landscape.

3.1.2.1. Nab experiment at the Spallation Neutron Source. The Nab experiment at the SNS aims to make precision measurements of a with a relative uncertainty of 1×10^{-3} and b with an absolute uncertainty of 3×10^{-3} (39). The experiment will utilize the cold neutron beam on the FnPB (37) to detect protons and electrons in coincidence for a measurement of a, as well as the electron energy spectrum for b.

The Nab spectrometer will guide charged neutron decay particles (protons and electrons) to large-area, segmented silicon detectors (89) at the bottom and top of the spectrometer. The protons can be detected in the upper detector only, while electrons can be detected in both detectors. The experimental design requires knowledge of electron energy (reconstructed for a single decay) as well as proton momentum (reconstructed from the time of flight relative to electron detection). To estimate the proton momentum from the proton time of flight, the Nab magnet utilizes a long asymmetric magnetic spectrometer, so that protons travel along a 5-m path and enter the top detector fully longitudinalized (meaning that the proton momentum is normal to the face of the detector). The magnetic filter at beam height in **Figure 6** excludes the proton trajectories that will not meet this longitudinalization condition. Additionally, the upper detector will be held at a potential of -30 keV so as to accelerate the protons to penetrate the dead layer of the detector. Simulations of protons and electrons in the spectrometer and detector are under vigorous study. The Nab experiment has been installed on the FnPB, and commissioning began in 2021. The Nab apparatus is well suited for follow-up measurements with a polarized cold neutron beam, such as the pNab experiment.

3.2. Matter/Antimatter Asymmetry

A new source of *CP* or *T* violation is one of the highest intellectual pursuits in nuclear, particle, and astrophysics, as more *CP* violation is needed to explain the baryon asymmetry of the Universe.

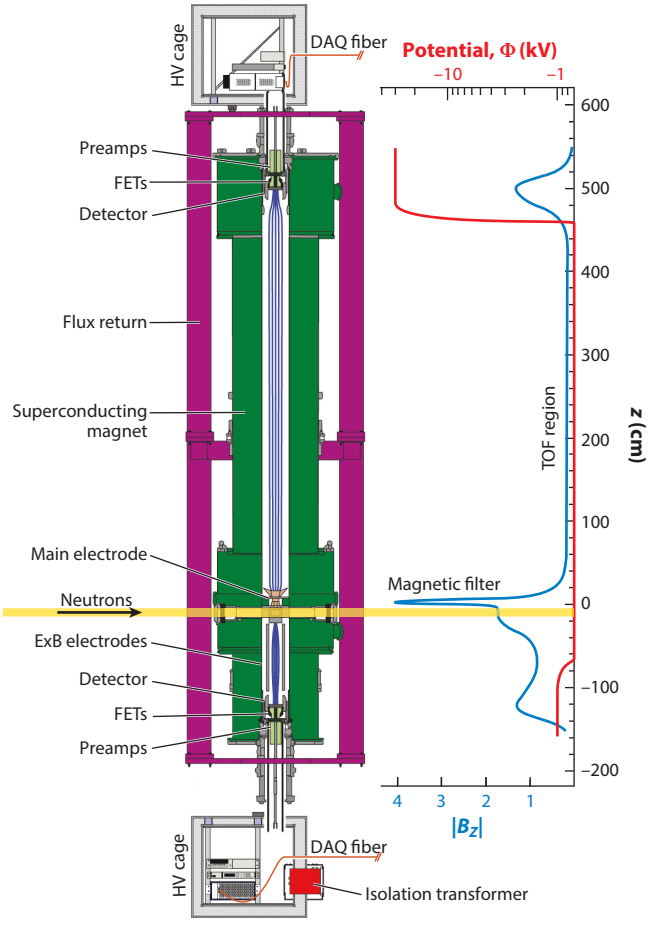

Figure 6

A model of the Nab spectrometer (for further details, see 39). The cryogenic superconducting magnet, oriented transversely to the neutron beamline, is shown in green. Purple denotes the magnet compensation package. The two detector packages are inside the magnet volume, with HV cages situated around the protrusion of each detector mount. The magnetic field magnitude in the z direction is shown on the right, along with the potential. Abbreviations: ExB, protons experiencing a force in the x direction from the interaction of electric (E) and magnetic (B) fields; FET, field-effect transistor; HV, high-voltage; TOF, time-of-flight. Figure adapted with permission from Reference 39.

Sakharov (90) suggests that *CP* violation, and thus TRV under the assumption of *CPT* invariance, is essential to produce the baryon asymmetry in Big Bang cosmology. Although *CP* violation and TRV were first observed in K and B mesons (91), the size of the violation was not enough to explain the baryon asymmetry determined from experimental observations. Thus, new sources of BSM *CP* violation and TRV are needed to explain the baryon asymmetry problem. Additionally, new sources of TRV in low-energy observables manifest in different ways, such that all TRV searches are not equally sensitive to all possible mechanisms (92, 93). To this end, it is necessary to search for TRV in multiple systems with sufficient and different sensitivity for a BSM signal. We discuss two types of searches for *CP* violation and TRV with neutrons: the search for a nonzero nEDM and the search for TRV terms in the forward-scattering amplitude in neutron interactions in compound heavy nuclei.

3.2.1. Neutron electric dipole moment searches. The search for a nonzero nEDM is quite compelling, as the neutron is the simplest and theoretically cleanest neutral, long-lived hadronic system with which to conduct such a measurement. Current SM estimates of the nEDM are on the scale of 10^{-32} e·cm, which is attributed to the *CP*-violating phase in the CKM matrix, δ_{CKM}. The most recent experimental limit, $d_n < 1.8 \times 10^{-26}$ e·cm (90% CL) (54), is still six orders of magnitude away from the SM prediction, leaving a large phase space for BSM models to exist. The goal of next-generation nEDM experiments is to increase the sensitivity by a factor of 10 to 100 (34, 40, 94).

Between the current nEDM limit and the SM prediction is a fertile area for BSM physics to induce the *CP* violation required to generate the baryon asymmetry in the Universe. Constraints can be placed on the parameters of minimal supersymmetric models, two-Higgs-doublet models, left–right symmetric models, and others as the limit on nEDM is reduced (93). To be consistent with the observed baryon asymmetry of the Universe, some of these BSM models predict a nonzero nEDM larger than the 10^{-28} e·cm. As a consequence, the next-generation experiments targeting this sensitivity level will be poised for discovery or will significantly constrain the models. Electron and nuclear EDM searches are also pushing their limits toward discovery. A discovery in a single system will not unambiguously determine its origin, and EDM searches in all of these systems should be viewed as complementary.

3.2.1.1. nEDM@SNS experiment. The nEDM@SNS experiment (40, 68) aims to reach a precision of 10^{-28} e·cm. The technique involves measuring the Larmor precession frequency of neutrons, ω_n, with the magnetic moment (μ_n) aligned in the plane perpendicular to a static magnetic field (B_0) and a static electric field (E_0) applied parallel/antiparallel to B_0 (32). The nEDM, d_n, enters the expression in the following way:

$$\omega_n = \frac{-2(\mu_n B_0 \pm d_n E_0)}{\hbar}. \qquad 12.$$

The statistical sensitivity of the experiment is driven by three factors: the strength of the applied electric field (E_0), the number of neutrons precessing (N), and the precession measurement time (τ):

$$\sigma_{d_n} \approx \frac{1}{E_0 \tau \sqrt{N}}. \qquad 13.$$

The N in the denominator refers specifically to spin-polarized neutrons. UCNs will be produced via superthermal scattering of incoming polarized 8.9-Å cold neutrons from photons in superfluid ^{4}He, enabling applications of large electric fields. The measurement will employ an admixture of ^{3}He, which will precess along with the neutrons but at a different frequency, leading to occasional capture. The energy released from the decay products of this capture will be transferred to the liquid helium and produce UV scintillation light, where the rate of scintillation will vary with the applied electric and magnetic fields. This rate can be used to extract the Larmor precession frequency and the nEDM. **Figure 7** depicts the apparatus. The figure shows the design elements intended to shield against external fields, such as external field cancellation coils and both room-temperature and superconducting shielding. The nEDM@SNS Collaboration expects to begin taking neutron data in 2027.

3.2.1.2. n2EDM experiment at the Paul Scherrer Institute. In 2020, the PSI nEDM experiment completed an improved search using an upgraded version of the RAL-ILL-Sussex apparatus (53), which reduced the upper limit to $d_n < 1.8 \times 10^{-26}$ e·cm (54). This effort demonstrated both that the PSI UCN source was capable of providing a sufficient UCN density to improve the statistical sensitivity and that the magnetic field nonuniformities could be assessed through the

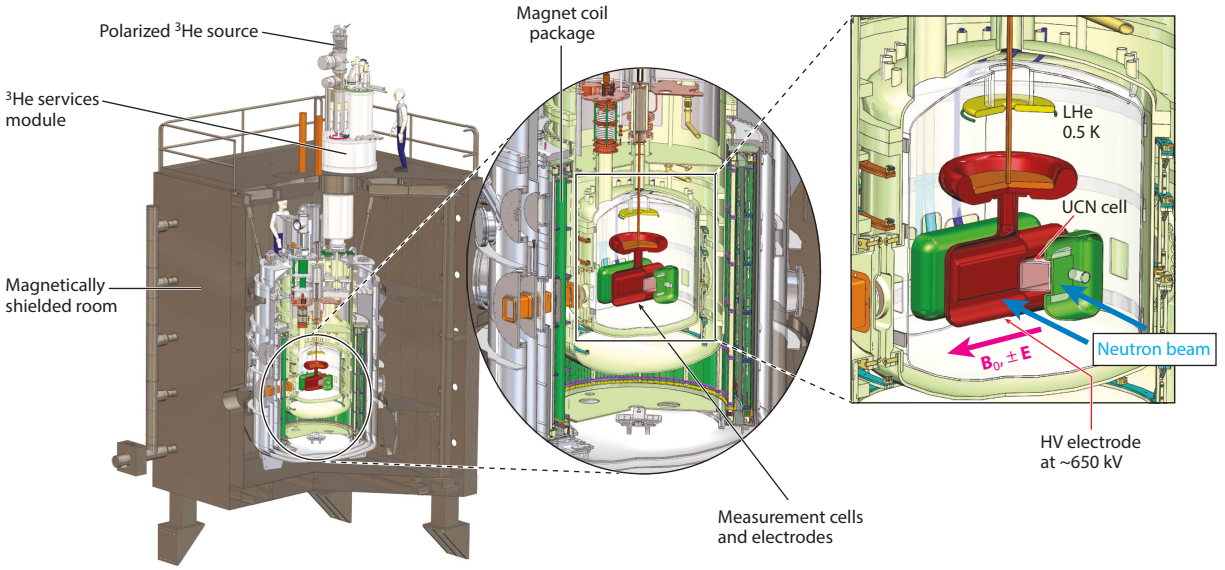

Figure 7

Schematic of the nEDM@SNS experimental apparatus (for details, see 68).

addition of an array of 15 external cesium magnetometers at high precision to significantly reduce the impact on the systematic uncertainty budget.

A room-temperature double-cell experiment currently under development will improve both the statistical and systematic precision, with a design sensitivity of 10^{-27} e·cm (96) (**Figure 8**). In the double-cell configuration, the boundary between cells is held at a positive electric potential while the opposite side of the cell is grounded, creating an electric field that is oriented parallel to the UCN spin in one cell and antiparallel in the other. This configuration allows simultaneous measurements of precession with the spin aligned and antialigned with the electric field, which can aid in the cancellation of time-dependent systematic effects. Another advantage is that more UCNs are loaded into the experiment per fill cycle. A six-layer magnetically shielded room with active compensation will be used to maintain a stable magnetic environment. The n2EDM experiment is expected to reach its precision goal in 500 days of data taking.

3.2.1.3. nEDM experiment at Los Alamos Neutron Science Center. Construction of a room-temperature nEDM search at the LANSCE UCN source began in 2014 (**Figure 9**). The first step was an upgrade of the UCN source to enable statistical sensitivity of 3×10^{-27} e·cm after 5 years (34). This effort will also use a double-precession-cell geometry to perform a Ramsey separated oscillatory field–style measurement (97) with a mercury comagnetometer and an array of external magnetometers. A multilayer magnetically shielded room with active compensation was installed in 2021, and the experiment will begin commissioning and initial testing in 2022.

3.2.1.4. TRIUMF. Having successfully demonstrated the production of UCNs at its source, the TRIUMF nEDM Collaboration is developing a new liquid helium source and a room-temperature nEDM experiment. The upgraded source is expected to load the double-cell geometry with a density of 300 UCNs cm^{-3}, which will enable a 10^{-27} e·cm level measurement in 400 operating days (57). A multilayer magnetically shielded room will be installed in 2022, and construction and commissioning of the nEDM experiment will start the following year.

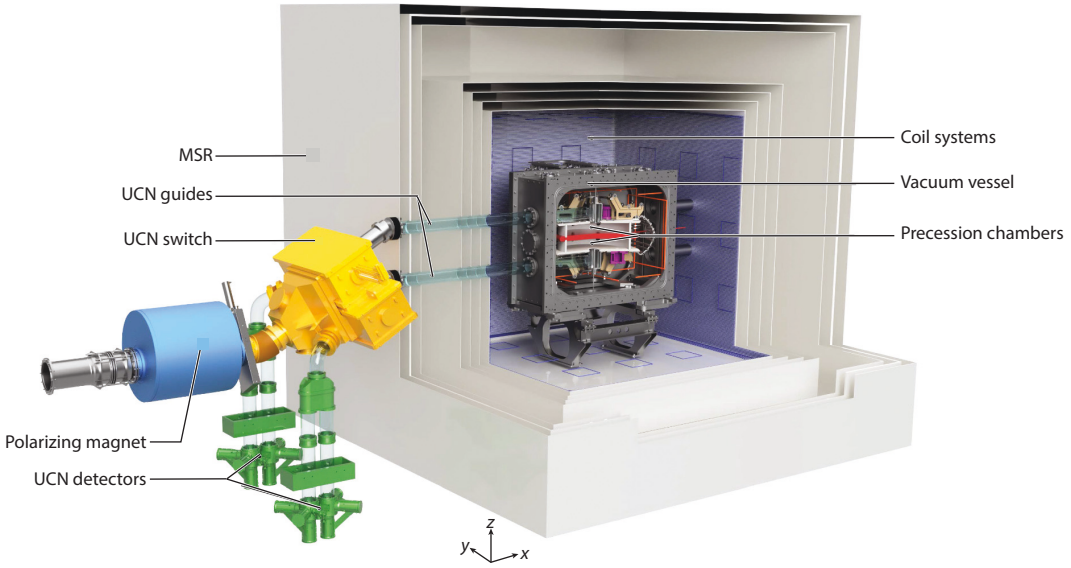

Figure 8

Schematic of the n2EDM apparatus at PSI (for design details, see 95). Abbreviations: MSR, magnetically shielded room; UCN, ultracold neutron. Figure adapted with permission from Reference 95.

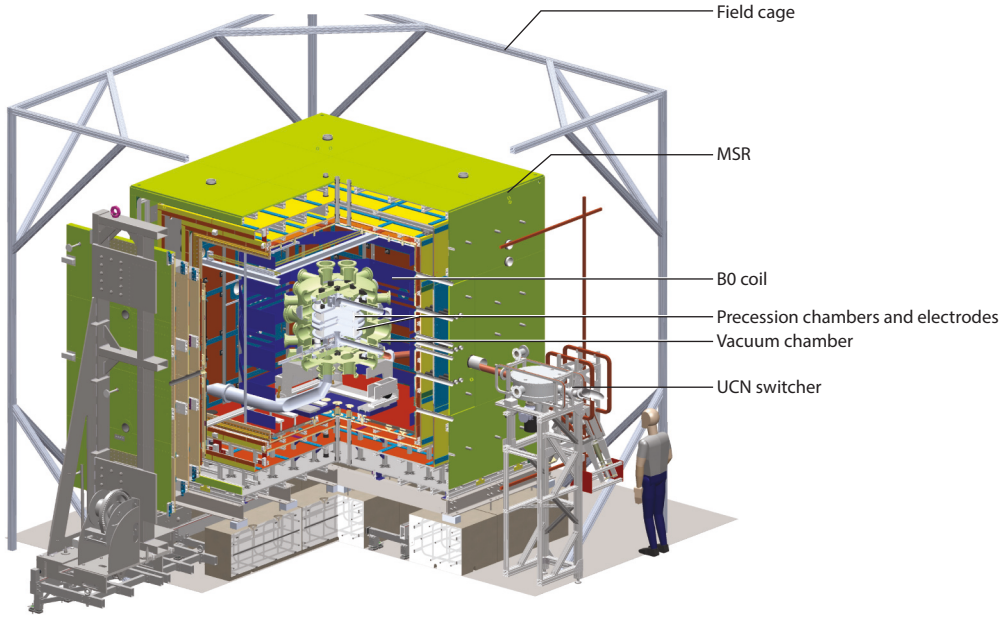

Figure 9

A schematic of the LANSCE nEDM experiment. A double precession chamber system is placed inside a nonmagnetic vacuum chamber, which in turn is placed inside an MSR with a shielding factor exceeding 10^5 at 0.01 Hz. A gapped solenoid coil system provides a uniform 1-μT magnetic field. Abbreviation: MSR, magnetically shielded room; nEDM, electric dipole moment of the neutron; UCN, ultracold neutron.

3.2.2. Time-reversal violation in neutron–nucleus interactions. The search for TRV through other types of mechanisms has been ongoing for decades, but only in the last few years have TRV experiments with neutron–nucleus interactions with sufficient precision been realized; they are now rapidly developing (98, 99). In addition, the sensitivity of neutron–nucleus experiments is complementary to the search for a nonzero nEDM. The basic concept of searching for TRV in the neutron–nucleus system is to isolate the T-odd term in the forward-scattering amplitude $f(0)$ of polarized neutrons on polarized targets:

$$f(0) = A + B\,\sigma_n \cdot \mathbf{I}_N + C\,\sigma_n \cdot \mathbf{k}_n + D\,\mathbf{I}_N \cdot \mathbf{k}_n + E\,\sigma_n \cdot (\mathbf{k}_n \times \mathbf{I}_N). \quad 14.$$

The term $E\,\sigma_n \cdot (\mathbf{k}_n \times \mathbf{I}_N)$ involves the cross product of the neutron spin σ_n, neutron momentum $\mathbf{k}_n$, and the target spin $\mathbf{I}_N$ and is both parity- and time-odd. An observable produced in a time-odd transformation can be constructed by reversing the direction of the neutron momentum and both spins. Effectively, one can reverse the direction of the neutron beam and spins to extract time-odd information (**Figure 10**).

The Neutron Optics Parity and Time Reversal (NOPTREX) Collaboration will conduct a sensitive search for TRV in polarized neutron transmission through polarized nuclei, exploiting properties of low-energy neutron–nucleus resonances that amplify TRV. Certain nuclei exhibit amplification of up to 10^6, providing high sensitivity to BSM physics and TRV.

In contrast to physics done with cold neutrons, epithermal neutrons are needed for neutron–nucleus resonances because of the energy regime of the resonances. Spallation sources with epithermal neutrons have recently been able to provide enough flux to carry out such studies, particularly at JSNS. With a combination of more epithermal flux, a proposed new measurement technique (98), and new theoretical developments (99), searches for both parity violation and TRV in heavy nuclei have resumed at LANSCE and JSNS. Future research will continue at LANSCE (at beamline FP12), JSNS (at beamlines BL04 and BL10), and possibly CSNS.

The TRIPLE Collaboration (100) was the first to prove that p-wave resonances of compound neutron–nucleus resonance reactions could be large enough to measure. The collaboration

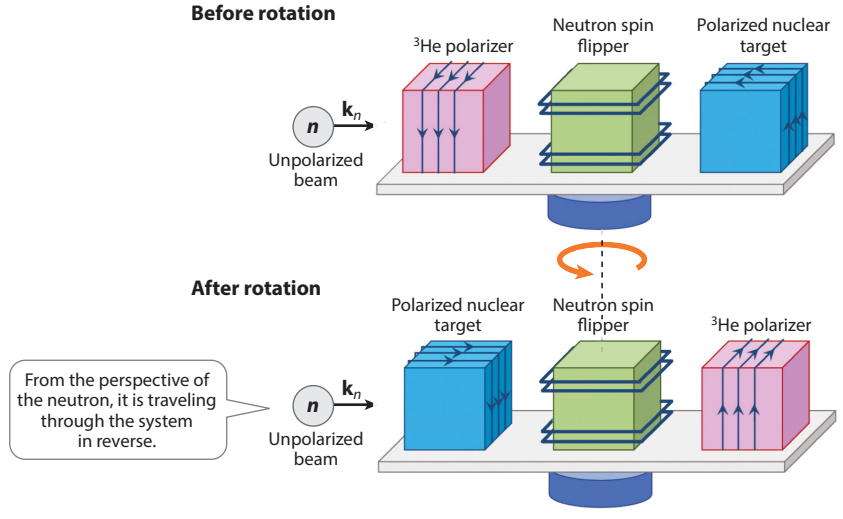

Figure 10

Conceptual diagram of spin reversal via rotation of the NOPTREX experimental apparatus. The apparatus is rotated 180° so that observables in the forward-scattering amplitude undergo a time-reversal inversion. Figure adapted from an image provided by Danielle Schaper.

measured approximately 80 different resonances in an experimental survey of heavy nuclei in a range that theoretically predicted large resonances at the time. Since then, improvements have revealed additional possible amplified resonances in a different regime, motivating the NOPTREX Collaboration to propose a search for parity violation in unmeasured heavy nuclei that could be new candidate nuclei for TRV.

3.3. The Hadronic Weak Interaction

The weak interaction can be generally categorized into three sectors: the leptonic interaction, the semileptonic interaction, and the HWI. The underlying mechanisms of the leptonic and semileptonic interactions are understood but are still under vigorous experimental investigation, such as neutron β decay (as discussed in Section 3.1). The third sector, the HWI, is not as well understood because weak interactions between hadrons occur at a scale where internal structure and the strong interaction between quarks compete with the weak interaction. The strong interaction at low energies involves the poorly understood nonperturbative QCD, complicating the HWI (101). The range of the quark–quark weak interaction is ∼100 times smaller than the strong interaction, so the HWI must contain nonperturbative QCD physics (102). The HWI can be thought of as an inside-out probe of QCD (103). Quark–quark interactions must abide by both weak and strong interactions, so any deviation from SM predictions must be connected to strong QCD (103). Thus, the HWI has the potential to shed light on quark–quark correlations in the nonperturbative limit of QCD while accessing the underlying weak interaction at the nucleon level, as predicted by the SM (101).

The typical strong interaction matrix element is a factor of 10^6 larger than its weak counterpart. Experiments can isolate the HWI in interactions between nucleons by utilizing parity—the strong interaction conserves parity, and the weak interaction violates it. Experiments using low-energy neutrons can exploit parity-violating terms in the forward-scattering amplitude in various systems to extract coupling constants in an HWI theoretical framework.

The theoretical benchmark of the HWI is a meson exchange model derived by Desplanques, Donoghue, and Holstein (the DDH model) (104). This model describes the low-energy nucleon–nucleon interaction through pseudoscalar and vector mesons, which couple a weak vertex to a strong vertex. The meson exchange forms a potential that can be described by seven parity-violating couplings, h_π^1, $h_\rho^{0,1,1',2}$, and $h_\omega^{0,1}$, through the meson exchange (subscript) and isospin change (superscript) (104). The DDH model offers predictions for the couplings in the form of reasonable ranges, which can be translated into central values with ∼100% uncertainties. Although this framework basically estimates only the order of magnitude of the coupling constants, it has been an important means of analyzing experimental results (105). Subsequently, various model-independent effective field theories (EFTs) were developed (106–109). EFTs describe the HWI at low energy with five *S–P* wave transitions between two nucleons, forming five low-energy constants (LECs) even when using different phenomenology. Because the EFTs are model independent, the HWI can ultimately be described by these five LECs. Results using the $1/N_c$ QCD power counting method on these HWI theories give a better sense of the scale of the couplings to ∼30% when expanding the Hamiltonian up to $\mathcal{O}(1/N_c)$ (110, 111). Additionally, a leading-order analysis of the hierarchy of the couplings has been performed to help guide the next generation of low-energy experiments (112).

Low-energy, few-body experiments with neutrons can measure linear combinations of the LECs with high precision. The experiments can be roughly divided into two classes: (*a*) measurements of asymmetries in neutron capture on light nuclei and (*b*) measurements of neutron spin precession in light nuclei. A measurement of the circular polarization P_γ of γs emitted in

$n + p \rightarrow d + \gamma$ was performed in 1984 (113) at the 10^{-7} level, which does not contribute to the precision determination of the couplings of the current era. More recently, two neutron capture experiments, NPDGamma (38) and n–^{3}He (10), were carried out at the FnPB at the SNS. NPDGamma measured the spin angular asymmetry A_γ of γs in $\mathbf{n} + p \rightarrow d + \gamma$, which, for the most part, isolates the $\Delta I = 1$ channel, the h_π^1 coupling in the DDH model, and the $^3S_1 \rightarrow {}^3P_1$ transition in EFTs. The NPDGamma Collaboration (9) measured $A_\gamma = -3.0 \pm 1.4 \times 10^{-8}$, a result that is statistics limited. The n–^{3}He Collaboration (10) measured the longitudinal asymmetry A_L in the ^{3}He($\mathbf{n}$, p)^{3}H reaction, which is related to the $\Delta I = 0$, 1, and 2 channels; the h_π^1, $h_\rho^{0,1,2}$, and $h_\omega^{0,1}$ DDH couplings; and all the S–P transitions in the EFT LECs. The result was $A_{PV} = (1.58 \pm 0.97_{stat} \pm 0.24_{syst}) \times 10^{-8}$, yielding the smallest uncertainty in any parity-violation experiment. Along with the NPDGamma result, the n–^{3}He Collaboration (10) published a linear combination of the ρ and ω couplings. It is clear that additional few-body measurements are required to clear up the HWI landscape. Additionally, once the couplings have been determined, one can test the analysis of heavy nuclei resonances, as discussed in Section 3.2.2.

A possible experiment to help fully describe the HWI is the spin angular asymmetry A_γ of γs in $\mathbf{n} + d \rightarrow t + \gamma$ (NDTGamma), which is sensitive to the $\Delta I = 0$ and 1 channels, a combination that will complement the NPDGamma and n–^{3}He experiments. The asymmetry is expected to be somewhat larger as a result of the suppressed strong interaction in nD capture. This process suffers from a very low signal-to-noise ratio and requires a stricter discrimination from background to boost sensitivity. Unlike the NPDGamma and n–^{3}He experiments, which were performed in current mode, NDTGamma must be a counting-mode experiment. Its digital pulse processing and data acquisition needs could be met with new technology, and NDTGamma plans to make feasibility and R&D measurements at LANSCE in the near future and assess possibilities at the ESS.

Another possible set of HWI experiments with neutrons involves neutron spin rotation (NSR). NSR ($d\phi/dz$) has been measured in the α system, limited by statistics (114). The NSR Collaboration plans to measure $d\phi/dz$ in $\mathbf{n} + \alpha \rightarrow \mathbf{n} + \alpha$ in liquid helium at the NIST Center for Neutron Research to higher precision than previously measured. NSR in the α system is proportional to the $\Delta I = 0$ and 1 channels, complementary to both n–^{3}He and NPDGamma. Spin rotation in p and d presents difficult systematic uncertainties to overcome but could be performed at future higher-flux spallation sources such as ESS. Because NSR measurements typically require higher neutron fluxes than spallation sources, previous measurements were performed at reactors.

4. OUTLOOK

For more than 70 years, low-energy neutrons have been an extremely productive tool for the investigation of fundamental interactions. However, because nearly all of the most interesting studies have been statistically limited, it is not surprising that progress has been closely coupled to advances in available fluxes, and we expect this situation to continue. For investigations with cold neutrons, the ESS (under construction) will provide much higher pulsed beam intensities than are currently available. While there are no immediate plans for a fundamental physics program at the ESS, the issue is under active consideration. For UCNs, the use of dedicated spallation target moderator systems (such as those in operation at PSI and LANSCE) has been extremely productive, and it is likely that much higher densities of UCNs will become available as such sources are fully optimized. Another opportunity that has yet to be fully exploited is the integration of the UCN source and experimental volume, as has been proposed for the nEDM@SNS experiment. Realization of these opportunities as well as continuing exploitation of spallation source cold neutron beams offers the prospect of a least a decade's worth of exciting results.

DISCLOSURE STATEMENT

The authors are not aware of any affiliations, memberships, funding, or financial holdings that might be perceived as affecting the objectivity of this review.

ACKNOWLEDGMENTS

We thank Mike Snow for his encyclopedic knowledge and Chien Yeah Seng for his helpful comments. The writing of this review was supported in part by the US Department of Energy, Office of Science, Office of Nuclear Physics (contract DE-FG02-03ER41258), and by the National Science Foundation (contract OIA-1849213, subaward 3200002692-21-336).

LITERATURE CITED

1. Rutherford E. *Proc. R. Soc. A* 97:374 (1920)
2. Snell AH, Pleasonton F, McCord RV. *Phys. Rev.* 78:310 (1950)
3. Smith JH, Purcell EM, Ramsey NF. *Phys. Rev.* 108:120 (1957)
4. Fermi E. *Nuovo Cim.* 9:1 (1934)
5. Pauli W. Letter presented at the Gauverein Meeting, Tübingen, Ger., Dec. 4. **https://fermatslibrary.com/s/the-proposal-of-the-neutrino** (1930)
6. Salam A. *Conf. Proc. C* 680519:367 (1968)
7. Feynman RP, Gell-Mann M. *Phys. Rev.* 109:193 (1958)
8. Weinberg S. *Phys. Rev. Lett.* 19:1264 (1967)
9. Blyth D, et al. *Phys. Rev. Lett.* 121:242002 (2018)
10. Gericke M, et al. *Phys. Rev. Lett.* 125:131803 (2020)
11. Maier-Leibnitz H, Springer T. *Annu. Rev. Nucl. Sci.* 16:207 (1966)
12. Trinks U, Hartmann J, Paul S, Schott W. *Nucl. Instrum. Methods A* 440:666 (2000)
13. Rauch H, Werner SA. *Neutron Interferometry: Lessons in Experimental Quantum Mechanics, Wave–Particle Duality, and Entanglement.* Oxford, UK: Oxford Scholarsh. Online. 2nd ed. (2015)
14. Byrne J. *Neutrons, Nuclei and Matter: An Exploration of the Physics of Slow Neutrons.* New York: Dover (1994)
15. Krupchitsky PA. *Fundamental Research with Polarized Slow Neutrons.* Berlin/Heidelberg: Springer (1987)
16. Steyerl A, et al. *Phys. Lett. A* 116:347 (1986)
17. Abele H. *Prog. Part. Nucl. Phys.* 60:1 (2008)
18. Shahi C, et al. *Nucl. Instrum. Methods A* 813:111 (2016)
19. Greene G, Arif M, Dewey M, Snow W. *J. Res. Natl. Inst. Stand. Technol.* 98:135 (1993)
20. Nico J, et al. *Phys. Rev. C* 71:055502 (2005)
21. Yue A, et al. *Phys. Rev. Lett.* 111:222501 (2013)
22. Hassan MT, et al. *Phys. Rev. C* 103:045502 (2021)
23. Hoogerheide SF, et al. *Eur. Phys. J. Web Conf.* 219:03002 (2019)
24. Bales MJ, et al. *Phys. Rev. Lett.* 116:242501 (2016)
25. Bensussan A, Salome J. *Nucl. Instrum. Methods* 155:11 (1978)
26. Guerrero C, et al. *Eur. Phys. J. A* 49:1 (2013)
27. Shvetsov VN. *Quantum Beam Sci.* 1:6 (2017)
28. Flaska M, et al. *Nucl. Instrum. Methods A* 555:329 (2005)
29. Barbeau PS, Efremenko Y, Scholberg K. arXiv:2111.07033 [hep-ex] (2021)
30. Musgrave M, et al. *Nucl. Instrum. Methods A* 895:19 (2018)
31. Golub R, Richardson D, Lamoreaux S. *Ultra-Cold Neutrons.* New York: Hilger (1991)
32. Golub R, Lamoreaux SK. *Phys. Rep.* 237:1 (1994)
33. Saunders A, et al. *Rev. Sci. Instrum.* 84:013304 (2013)
34. Ito TM, et al. *Phys. Rev. C* 97:012501 (2018)
35. Lauss B, Blau B. *SciPost Phys. Proc.* 5:004 (2021)

36. Anghel A, et al. *Nucl. Instrum. Methods A* 611:272 (2009)
37. Fomin N, et al. *Nucl. Instrum. Methods A* 773:45 (2015)
38. Blyth D, et al. *Phys. Rev. Lett.* 121:242002 (2018)
39. Fry J, et al. *Eur. Phys. J. Web Conf.* 219:04002 (2019)
40. Ahmed M, et al. *J. Instrum.* 14:P11017 (2019)
41. Seo PN, et al. *Nucl. Instrum. Methods A* 517:285 (2004)
42. Gericke MT, et al. *Phys. Rev. C* 83:015505 (2011)
43. Wagner W, et al. *Nucl. Instrum. Methods A* 562:541 (2006)
44. Geue T, et al. *Neutron News* 32:37 (2021)
45. Sheng W, et al. *Chin. Phys. C* 33:1 (2009)
46. Chin. Acad. Sci. *First neutron beam produced: a great milestone for China Spallation Neutron Source.* News Release, CSNS, Chin. Acad. Sci., Dongguan, China, Sept. 6. **https://phys.org/news/2017-09-neutron-great-milestone-china-spallation.html** (2017)
47. Chin. Acad. Sci. *The accelerator.* News Release, CSNS, Chin. Acad. Sci., Dongguan, China, March 10. **http://english.ihep.cas.cn/csns/fa/ac/202109/t20210910_283138.html** (2017)
48. Chin. Acad. Sci. *BL12: neutron physics and application spectrometer* (*planning*). News Release, CSNS, Chin. Acad. Sci., Dongguan, China, May 19. **http://english.ihep.cas.cn/csns/fa/in/202109/t20210915_283268.html** (2021)
49. Parnell SR, et al. *Phys. Rev. D* 101:122002 (2020)
50. Ignatovich V. *The Physics of Ultracold Neutrons.* Oxford, UK: Oxford Univ. Press (1991)
51. Gonzalez FM, et al. *Phys. Rev. Lett.* 127:162501 (2021)
52. Brown MAP, et al. *Phys. Rev. C* 97:035505 (2018)
53. Pendlebury JM, et al. *Phys. Rev. D* 92:092003 (2015)
54. Abel C, et al. *Phys. Rev. Lett.* 124:081803 (2020)
55. Jenke T, Geltenbort P, Lemmel H, Abele H. *Nat. Phys.* 7:468 (2011)
56. Young AR, et al. *J. Phys. G* 41:114007 (2014)
57. Martin J, et al. *Nucl. Phys. News* 31:19 (2021)
58. Tang Z, et al. *Rev. Sci. Instrum.* 92:023305 (2021)
59. Pattie RW Jr., et al. *Nucl. Instrum. Methods A* 872:64 (2017)
60. Becker H, et al. *Nucl. Instrum. Methods A* 777:20 (2015)
61. Anghel A, et al. *Eur. Phys. J. A* 54:148 (2018)
62. Bison G, et al. *Phys. Rev. C* 95:045503 (2017)
63. Baker C, et al. *Nucl. Instrum. Methods A* 736:184 (2014)
64. Golub R, Pendlebury J. *Phys. Lett. A* 62:337 (1977)
65. Imajo S, et al. *Prog. Theor. Exp. Phys.* 2016:1 (2016)
66. Santoro V, et al. *J. Neutron Res.* 22:209 (2020)
67. O'Shaughnessy CM, et al. *Nucl. Instrum. Methods A* 611:171 (2009)
68. Leung K, et al. *Eur. Phys. J. Web Conf.* 219:02005 (2019)
69. González-Alonso M, Naviliat-Cuncic O, Severijns N. *Prog. Part. Nucl. Phys.* 104:165 (2019)
70. Hardy JC, Towner IS. *Phys. Rev. C* 102:1 (2020)
71. Seng CY, Gorchtein M, Ramsey-Musolf MJ. *Phys. Rev. D* 100:013001 (2019)
72. Seng CY, Gorchtein M, Patel HH, Ramsey-Musolf MJ. *Phys. Rev. Lett.* 121:241804 (2018)
73. Seng CY, Feng X, Gorchtein M, Jin LC. *Phys. Rev. D* 101:111301 (2020)
74. Hayen L. *Phys. Rev. D* 103:113001 (2021)
75. Pattie RW Jr., et al. *Science* 360:627 (2018)
76. Serebrov AP, et al. *Phys. Rev. C* 97:055503 (2018)
77. Robson JM. *Phys. Rev.* 83:349 (1951)
78. Ezhov VF, et al. *JETP Lett.* 107:671 (2018)
79. Materne S, et al. *Nucl. Instrum. Methods A* 611:176 (2009)
80. Roß KU. *Towards a high precision measurement of the free neutron lifetime with SPECT.* PhD Thesis, Johannes Gutenberg Univ., Mainz, Ger. (2021)
81. Zyla P, et al. *Prog. Theor. Exp. Phys.* 2020:083C01 (2020)

82. Byrne J, et al. *Nucl. Instrum. Methods A* 284:116 (1989)
83. Nagakura N, et al. *Eur. Phys. J. Web Conf.* 219:03003 (2019)
84. Hirota K, et al. *Prog. Theor. Exp. Phys.* 2020:123C02 (2020)
85. Sumi N, et al. *Phys. Soc. Jpn. Conf. Proc.* 33:011056 (2021)
86. Jackson J, Treiman S, Wyld H. *Phys. Rev.* 106:517 (1957)
87. Märkisch B, et al. *Phys. Rev. Lett.* 122:242501 (2019)
88. Zyla PA, et al. *Prog. Theor. Exp. Phys.* 2020:083C01 (2020)
89. Broussard LJ, et al. *Nucl. Instrum. Methods A* 849:83 (2017)
90. Sakharov AD. *Pis'ma Zh. Eksp. Teor. Fiz.* 5:32 (1967)
91. Christenson JH, Cronin JW, Fitch VL, Turlay R. *Phys. Rev. Lett.* 13:138 (1964)
92. Engel J, Ramsey-Musolf MJ, van Kolck U. *Prog. Part. Nucl. Phys.* 71:21 (2013)
93. Chupp T, Ramsey-Musolf M. *Phys. Rev. C* 91:035502 (2015)
94. Ahmed S, et al. *Phys. Rev. C* 99:025503 (2019)
95. Ayres NJ, et al. *Eur. Phys. J. C* 81:512 (2021)
96. Abel C, et al. *Eur. Phys. J. Web Conf.* 219:02002 (2019)
97. Ramsey NF. *Phys. Rev.* 78:695 (1950)
98. Bowman JD, Gudkov V. *Phys. Rev. C* 90:065503 (2014)
99. Gudkov V, Shimizu HM. *Phys. Rev. C* 97:065502 (2018)
100. Mitchell G, Bowman J, Penttilä S, Sharapov E. *Phys. Rep.* 354:157 (2001)
101. Haxton WC, Holstein BR. *Prog. Part. Nucl. Phys.* 71:185 (2013)
102. Fry J. In *Recent Progress in Few-Body Physics: Proceedings of the International Conference on Few-Body Problems in Physics* (*FB22*), p. 461. Berlin: Springer (2020)
103. Snow W. *Eur. Phys. J. A* 24:119 (2005)
104. Desplanques B, Donoghue JF, Holstein BR. *Ann. Phys.* 124:449 (1980)
105. Adelberger EG, Haxton WC. *Annu. Rev. Nucl. Part. Sci.* 35:501 (1985)
106. Zhu SL, et al. *Nucl. Phys. A* 748:435 (2005)
107. Liu CP. *Phys. Rev. C* 75:065501 (2007)
108. Phillips DR, Schindler MR, Springer RP. *Nucl. Phys. A* 822:1 (2009)
109. Schindler M, Springer R. *Prog. Part. Nucl. Phys.* 72:1 (2013)
110. Phillips DR, Samart D, Schat C. *Phys. Rev. Lett.* 114:062301 (2015)
111. Schindler MR, Springer RP, Vanasse J. *Phys. Rev. C* 93:025502 (2016)
112. Gardner S, Haxton W, Holstein BR. *Annu. Rev. Nucl. Part. Sci.* 67:69 (2017)
113. Knyaz'kov V, et al. *Nucl. Phys. A* 417:209 (1984)
114. Swanson HE, et al. *Phys. Rev. C* 100:015204 (2019)

Annual Review of Nuclear and Particle Science

Volume 72, 2022

Contents

Errata

An online log of corrections to *Annual Review of Nuclear and Particle Science* articles may be found at http://www.annualreviews.org/errata/nucl